Available online at www.sciencedirect.com
SCIENCE DIRECT®
Polymer 45 (2004) 2001–2015
polymer
www.elsevier.com/locate/polymer

A comparative study of melt spun polyamide-12 fibres reinforced with carbon nanotubes and nanofibres

J.K.W. Sandler[a], S. Pegel[a,b], M. Cadek[c], F. Gojny[b], M. van Es[d], J. Lohmar[e], W.J. Blau[c], K. Schulte[b], A.H. Windle[a], M.S.P. Shaffer[f,*]

[a]*Department of Materials Science and Metallurgy, University of Cambridge, Cambridge CB2 3QZ, UK*
[b]*Polymer Composites, Technical University Hamburg-Harburg, Hamburg D-21073, Germany*
[c]*Department of Physics, Materials Ireland Polymer Research Centre, University of Dublin-Trinity College, Dublin 2, Ireland*
[d]*DSM Research, Geleen 6160 MD, The Netherlands*
[e]*Degussa AG, Marl D-45764, Germany*
[f]*Department of Chemistry, Imperial College London, Imperial College Road, London SW7 2AZ, UK*

Received 23 September 2003; received in revised form 23 December 2003; accepted 15 January 2004

Abstract

A range of multi-wall carbon nanotubes and carbon nanofibres were mixed with a polyamide-12 matrix using a twin-screw microextruder, and the resulting blends spun to produce a series of reinforced polymer fibres. The aim was to compare the dispersion and resulting mechanical properties achieved for nanotubes produced by the electric arc and a variety of chemical vapour deposition techniques. A high quality of dispersion was achieved for all the catalytically-grown materials and the greatest improvements in stiffness were observed using aligned, substrate-grown, carbon nanotubes. The use of entangled multi-wall carbon nanotubes led to the most pronounced increase in yield stress, most likely as result of increased constraint of the polymer matrix due to their relatively high surface area. The degrees of polymer and nanofiller alignment and the morphology of the polymer matrix were assessed using X-ray diffraction and differential scanning calorimetry. The carbon nanotubes were found to act as nucleation sites under slow cooling conditions, the effect scaling with effective surface area. Nevertheless, no significant variations in polymer morphology as a function of nanoscale filler type and loading fraction were observed under the melt spinning conditions applied. A simple rule-of-mixture evaluation of the nanocomposite stiffness revealed a higher effective modulus for the multi-wall carbon nanotubes compared to the carbon nanofibres, as a result of improved graphitic crystallinity. In addition, this approach allowed a general comparison of the effective nanotube modulus with those of nanoclays as well as common short glass and carbon fibre fillers in melt-blended polyamide composites. The experimental results further highlight the fact that the intrinsic crystalline quality, as well as the straightness of the embedded nanotubes, are significant factors influencing the reinforcement capability.

Keywords: Nanocomposites; Nanotubes; Polymer fibres

1. Introduction

Natural materials such as bone, tooth and nacre are very effective examples of nanocomposites consisting of proteins and minerals. The concept of exploiting the unusual properties of nanoscale reinforcement has found widespread interest in the polymer field. In fact, some of these nanocomposites have been under investigation for many years and have long found their commercial applications. Carbon-black-filled rubber for automotive applications is an excellent example. Within the last decade, carbon nanotubes have stimulated considerable scientific interest due to their exciting physical and mechanical properties, which result from their unique microstructure. Recent experimental investigations have demonstrated the potential of carbon nanotubes as small volume fraction reinforcements in polymer matrix systems; for comprehensive reviews see Refs. [1,2].

The production of carbon nanotubes in large quantities, high purities, and with a uniform size still poses significant challenges, but an increasing number of companies are focussing on scaled-up synthesis routes. Although highly

* Corresponding author. Tel.: +44-20-7594-5825; fax: +44-20-7594-5801.
E-mail address: m.shaffer@imperial.ac.uk (M.S.P. Shaffer).

0032-3861/$ - see front matter © 2004 Published by Elsevier Ltd.
doi:10.1016/j.polymer.2004.01.023

crystalline materials can be most readily grown at high temperatures using electric arcs or laser ablation, large-scale synthesis efforts are mostly based on chemical vapour deposition (CVD) techniques that use moderate temperatures to decompose hydrocarbons over transition metals. The mechanical properties of individual multi-wall carbon nanotubes have been shown experimentally to depend strongly on the intrinsic crystalline quality of the material; the presence of stacking defects and pronounced structural disorder can reduce the elastic modulus by orders of magnitude [3]. Furthermore, CVD processes can lead to significant entanglement of the nanotubes. On the other hand, high-temperature growth processes such as the electric arc-discharge produce low nanotube volumes and purities. Although it is clearly important to select the appropriate nanotube material for a given application, very few systematic comparisons have been made.

The most promising current approaches towards increasing the orientation of nanoscale reinforcements within a matrix include optimisation of the extrusion die [4] and stretching the composite melt to form films [5–7] and fibres [8–14]. One complication is that the microstructure of semicrystalline thermoplastic polymer matrices is influenced not only by the processing history but also by the presence of nanoparticles. The addition of various types of carbon nanotubes and nanofibres to thermoplastics has already been observed to influence the crystallisation kinetics and resulting morphology [14–19]. Such changes in matrix morphology need to be considered when evaluating the nanocomposite performance with regard to the intrinsic filler properties [20,21]. The effects of carbon nanotubes or nanofibres on such oriented polymer systems, although significant [21], have not yet been fully established. Finally, it should be noted that the presence of additives such as colouring pigments has been shown to influence matrix morphology during fibre spinning [22], whilst there is the whole technology of nucleating agents which are deliberately added to influence crystalline microstructure.

To date, only relatively modest improvements in melt-blended nanotube composite strength and stiffness have been observed. These experimental results are probably symptomatic of the early stages of development of nanotube composite systems and have been explained in terms of a low level of dispersion, the use of intrinsically defective carbon material, and possibly poor intra-tube or interfacial shear strengths. A further critical issue is the shape of carbon nanotubes embedded in the polymer matrix. Carbon nanotube waviness may significantly reduce their reinforcement capability [23,24]. Since results to date, for large-scale CVD carbon nanotubes and nanofibres, do not yet indicate that the intrinsic mechanical properties are superior to conventional fillers, there is particular interest in using nanotubes in fine structures, such as spun fibres or micro-injection mouldings, where conventional chopped fibres cannot be physically accommodated. The approach used in this study explores this idea and was aimed at evaluating the reinforcement potential of a range of multi-wall carbon nanotubes in comparison to vapour-grown carbon nanofibres in as-spun polyamide-12 fibres. This approach allowed a range of filler loading fractions to be investigated using relatively small volumes of the various nanomaterials. Special emphasis was placed on the characterisation of the fillers' influence on the matrix crystallisation kinetics and the resulting polymer morphology.

2. Materials and experimental details

The arc-grown nanotubes (AGNT) [25], aligned catalytically-grown nanotubes (aCGNT) [26], and entangled catalytically-grown nanotubes (eCGNT) [27] were produced using previously reported techniques. The catalytically-grown nanofibres (CNF) were purchased from Applied Sciences Inc., USA, grade PR-19-PS. The average outer diameters of the nanomaterials were 15, 43, 10 and 155 nm, respectively. All materials were multi-walled and used as produced. All of the catalytically-grown materials were essentially pure except for the presence of the catalytic transition metal. The AGNT sample contained significant graphitic and nanoparticulate impurities, with a total nanotube weight content around 40% [25]. The matrix material was a polyamide-12, VESTAMID L1700, from Degussa. Linear aliphatic polyamides are semicrystalline polymers that usually exhibit a relatively high modulus, toughness and strength, low creep and good temperature resistance. They are used widely as engineering materials and fibres. Most commonly, polyamide-6 and 6,6 are used for commercial production of fibres for textile and engineering applications. Polyamide-12 fibres only represent a small fraction of the polyamide fibre market but exhibit an excellent strength/toughness balance.

The polymer pellets and carbon powders were weighed and dried, and then blended in a DSM twin-screw microextruder, operating at 220 °C at 80 rpm. The extrudate was roughly chopped and fed into a Rheometrics Scientific capillary rheometer also operating at 220 °C. A single strand was spun from a 1 mm diameter die, and wound up at around 0.5 m/s to produce a final fibre diameter targeted at 125 μm. Nanocomposites with a range of loading fractions up to 15 wt% were produced, depending on the availability of the nanofillers. Specifically, the following filler weight fractions were realised: 5, 10 and 15 wt% CNF, 1.25, 2.5 and 5 wt% aCGCNT, 1.25, 2.5 and 10 wt% AGNT, and 1.25, 2.5, 5 and 10 wt% eCGNT.

Thermal gravimetric analysis (TGA) was carried out using a Mettler TG50 thermal analysis unit. 10 mg of the PA12 nanocomposite fibres were placed into an aluminium oxide crucible and heated up in air (heating rate of 10 °C/min from 25 to 1000 °C under a constant air flow of 20 l/min). The samples were held initially at 100 °C for 1 hour, in order to remove any water present. Composite

samples were fractured under liquid nitrogen and mounted for observation in a JEOL 6430F FEG SEM, operating at 10 kV, after coating with chromium. 2D wide angle X-ray scattering (WAXS) fibre diffraction patterns were collected using Ni-filtered Cu Kα radiation on a Photonics CCD system and were calibrated using silicon powder. 1D X-ray diffraction data was collected on a Bruker (Siemens) D500 in transmission mode, using similar radiation. Individual fibre tensile testing was performed on a TA Instruments 2980 Dynamic Mechanical Analyzer applying a constant force ramp of 0.1 N/min, at 30 °C, with a gauge length of 5.5 mm, held between thin film clamps. At least 3 fibres were tested for each filler type and loading fraction, with the diameters measured for each sample. The maximum elongation that was achievable using this equipment was about 400%. Differential scanning calorimetry (DSC) was performed using a TA Instruments DSC 2920 operating at either 10 °C/min or 30 °C/min, between room temperature and 210 °C. Prior to the cooling runs, the samples were held isothermally at 210 °C for 5 minutes to erase the thermal history. Raman spectra were collected on a Renishaw micro-Raman system using a 50 × lens and a 25 mW argon laser (514 nm), with both the incident and backscattered light polarised parallel to the fibre axis.

3. Results

Macroscopically, all of the as-spun polyamide-12 nanocomposite fibres appeared to be of generally good quality, with a reasonable surface finish and uniform diameter, regardless of catalytic nanotube filler type and loading fraction. The entangled multi-wall carbon nanotubes led to a slightly rougher fibre surface compared to the carbon nanofibres and aligned multi-wall carbon nanotubes. Only the nanocomposite fibres containing the arc-grown multi-wall carbon nanotubes showed nonuniformity in diameter, which was independent of filler weight content. All nanocomposite fibres were coloured uniformly black.

Typical SEM images of the composite fibres are shown in Figs. 1 and 2, and demonstrate a high level of dispersion for all of the catalytically-grown materials, although occasional small aggregates were observed in the eCGNT samples. The AGNT showed a poor overall level of dispersion in all cases, with aggregates leading to the formation of voids within the fibres, as clearly evidenced by Fig. 1(d)). The quality of the dispersion across all the samples reflects the state of the nanotubes in the as-produced material. The arc-grown material is fused together by contaminating graphite, the eCGNTs separate well but retain some entanglements, whilst the straighter and unentangled aCGNTs and CNFs disperse most successfully. Maximum pull-out lengths appeared to be around 400–500 nm for both CNFs and eCGNTs but reached several microns for the aCGNT samples. The dispersed material with the highest crystallinity and straightness, the aCGNTs, gives the longest pull-out lengths, as might be expected. However, although the surfaces of the various CVD-grown nanotubes are expected to be similar, it is impossible at this stage to rule out the possibility of a particularly poor polymer-nanotube interaction or internal nanotube failures.

During thermogravimetric analysis, the CNFs and the aCGNTs showed similar behaviours, with a sharp weight loss on increasing temperature, peaking at about 600 °C. As an example, Fig. 3 shows the behaviour of the CNFs and the pure matrix. The main feature of the eCGNT data was similar, but there was an earlier weight loss of about 5% at 400 °C, suggesting the presence of a small amount of amorphous carbon. The AGNTs exhibited the highest temperature stability, with the maximum weight loss occurring at around 700 °C, reflecting the higher crystalline quality of the material. As can be seen in Fig. 3, the pure polymaide-12 matrix shows a two-stage decomposition process; a weight loss of about 10% occurs at 350 °C, followed by a second process centred at 450 °C. Both the CNFs and the aCGNTs stabilise the matrix against the first stage of degradation, even at low loading fractions. Similar effects have been observed previously in nanotube composites based on other polymers, and are thought to relate to radical capture by the nanotube surface [28]. The weights remaining after complete polymer decomposition are qualitatively consistent with the fraction of nanotubes present. Quantitatively, however, the values are distinctly low, presumably because most of the well-dispersed nanomaterials are physically lost from the sample as the polymer decomposes.

Comparative Raman spectra of the composites are shown in Fig. 4; the peaks associated with the carbon materials are much stronger than those of the matrix, due to resonance and absorbance effects. The two typical graphitic peaks can clearly be seen, the so-called G-peak, at $\sim 1585\ \mathrm{cm}^{-1}$, arising from the in-plane vibrations, and the D-peak, at $1350\ \mathrm{cm}^{-1}$, originating from disorder in the graphitic structure. The D/G intensity ratio is frequently used to assess the degree of crystallinity in carbon samples; a lower ratio indicates fewer defects in the crystal structure. The Raman data clearly reveal the differences in crystallinity between the various nanomaterials used. As might be expected, the arc-grown sample has the highest crystallinity, whilst the aCGNTs are significantly higher quality than the other catalytically-grown materials. A number of polymer peaks are clearly visible and identifiable by comparison with the pure polymer spectrum. They appear unaffected by the presence of the different nanofillers, although their intensity is low, and hence any subtle changes would be hard to identify.

Two-dimensional WAXS patterns of the extruded fibres are shown in Fig. 5, with examples of more detailed equatorial scans presented in Fig. 6. The two main features of the 2D patterns are an amorphous polymer halo and a crystalline diffraction ring at low angles. The amorphous halo is superimposed by a crystalline reflection in the

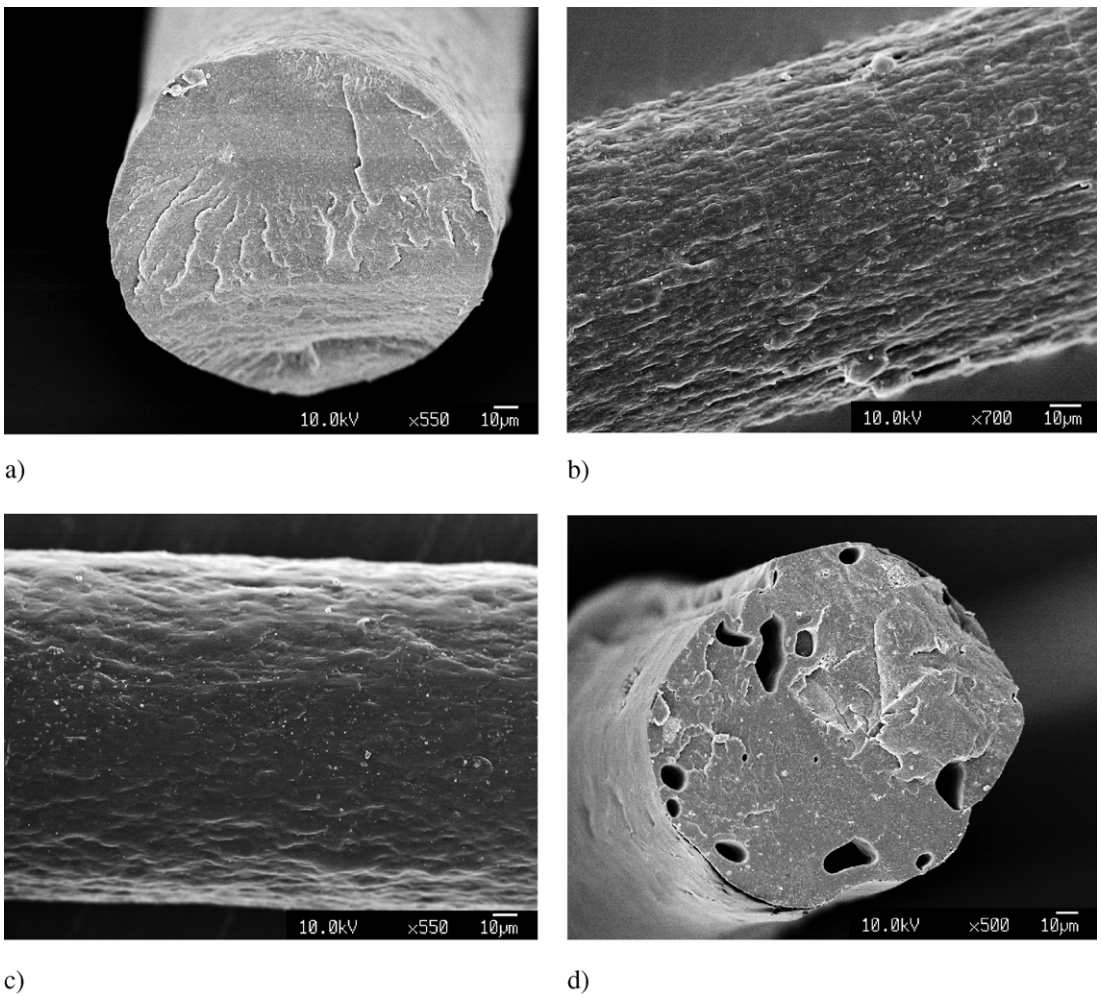

Fig. 1. SEM images of the nanocomposite fibres, containing (a) 10 wt% CNF, (b) 10 wt% eCGNT, (c) 5 wt% aCGNT, and (d) 5 wt% AGNT.

equatorial region, although the effect is more clearly seen in Fig. 6. These two reflections correspond to the γ-phase structure of polyamide-12. The graphitic (002) reflection of the carbon nanofibres and the aligned multi-wall nanotubes can be seen as semi-arcs (outermost, arrowed, reflection in Fig. 5(a) and (c)). The AGNT samples showed a random distribution of graphitic planes, consistent with the presence of equiaxed nanoparticles and aggregated nanotubes. Note the absence of any (002) reflection for the eCGNTs in Fig. 5(b), probably as a result of both their lower level of perfection (as indicated by the Raman data), and their smaller diameter.

There appears to be relatively little alignment of the polyamide-12 matrix in the as-spun fibres, although the increase in equatorial intensity indicates some orientation of the crystalline regions. Fig. 5(e) shows an example of a two-dimensional X-ray pattern obtained from a nanocomposite fibre bundle containing 5 wt% of the aCGNTs, strained to 100%. Clearly, there is now increased polymer alignment with the fibre axis and significant strain-induced crystallisation has occurred. The crystalline peaks are sharper and remain consistent with the γ-phase. In contrast, the alignment of the (002) reflections from the aCGNTs does not appear to be improved compared to Fig. 5(c).

Examples of equatorial line scans are shown in Fig. 6(a) for the pure polymer and the nanocomposite containing 5 wt% aCGNT, along with the results of 50:50 Lorentzian: Gaussian peak fittings. It can be seen that the polymer has a low crystallinity (amorphous halo centred at around $2\theta = 20.9°$, with a small crystalline peak superimposed on it at $2\theta = 21.5°$). In addition, analysis of the full width at half maximum (FWHM) of the crystalline peak revealed an increasing crystallite size for the nanotube filled samples, evidenced by a decreasing FWHM, with increasing filler loading fraction. As can be seen, in Fig. 6(b)), the effect is most prominent for low nanotube concentrations and levels off above 2.5 wt%, following a similar trend to the nucleation behaviour discussed below. Relatively little effect was observed for the CNF samples. The overall degree of crystallinity across all of the as-processed samples, as obtained from the X-ray patterns, was in the range 7-17%. This figure is an estimate, based, as it is, on the equatorial line scans which are influenced by differences in the polymer alignment. However, it represents an upper

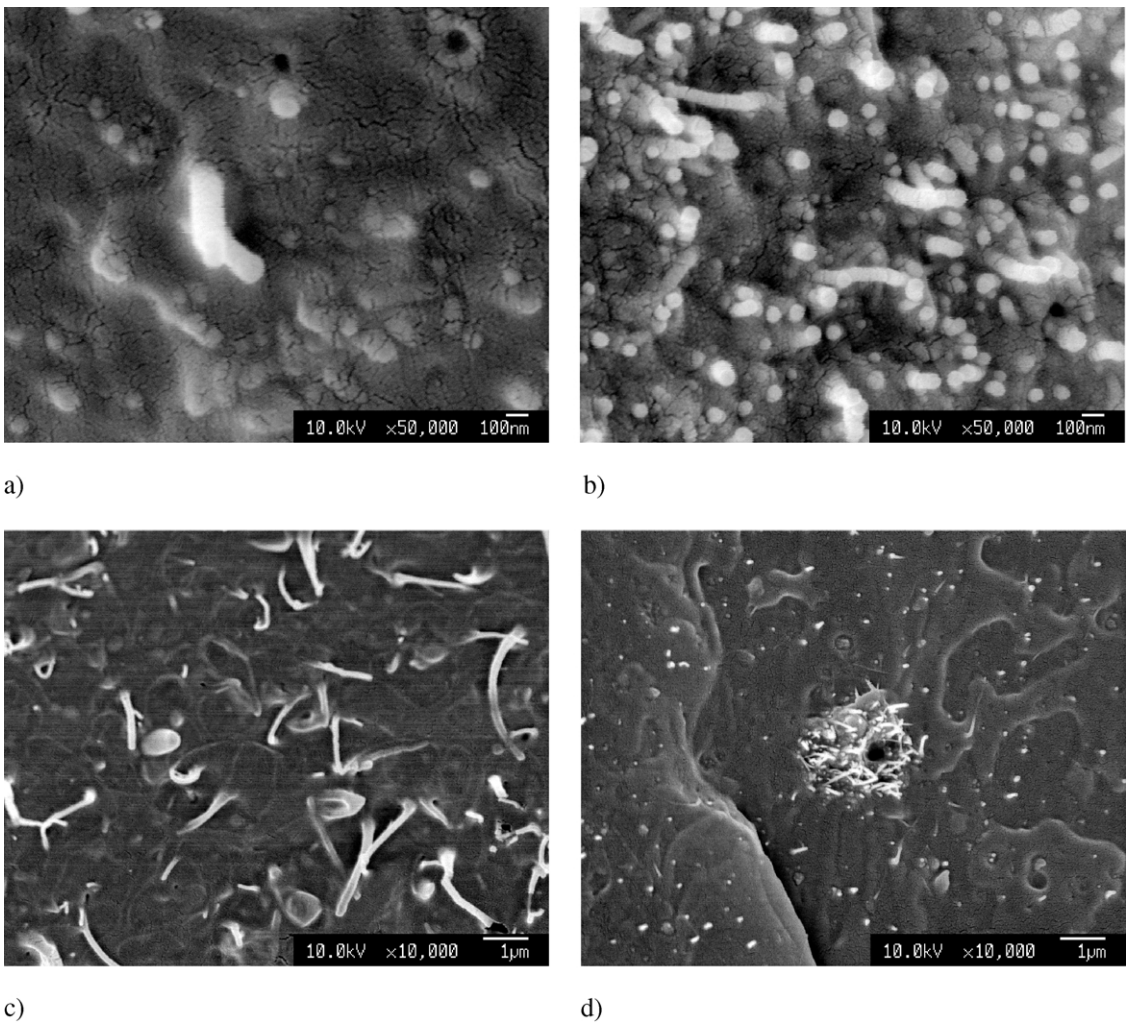

Fig. 2. Higher resolution SEM images of the nanocomposite fibres, containing (a) 10 wt% CNF, (b) 10 wt% eCGNT, (c) 5 wt% aCGNT, and (d) 5 wt% AGNT.

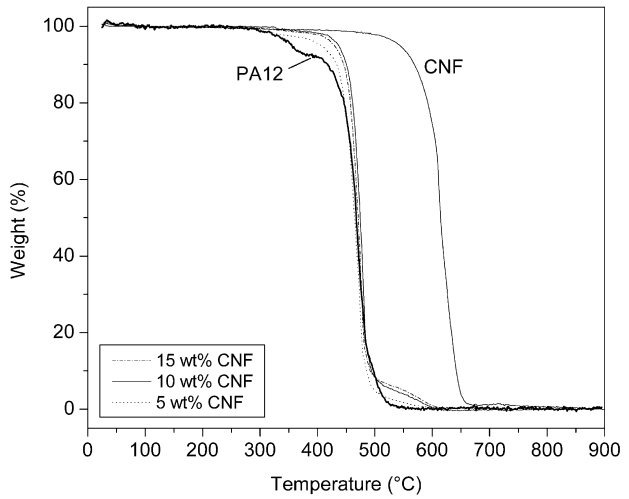

Fig. 3. Weight loss as a function of temperature for pure PA12 fibres and PA12 nanocomposite fibres containing various filler weight fractions of CNF.

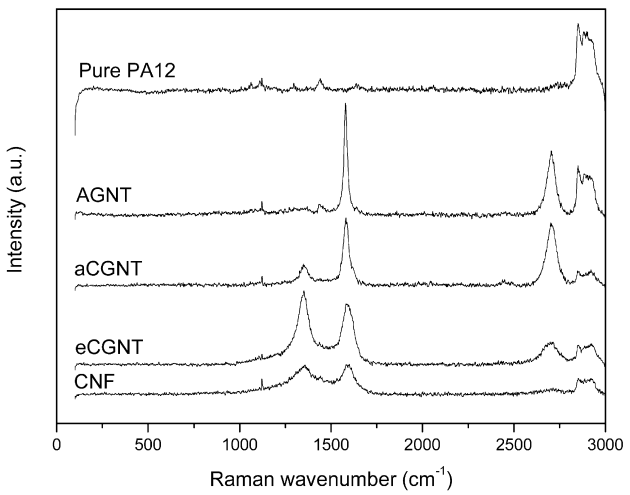

Fig. 4. Raman spectra of the pure polymer and nanocomposite fibres.

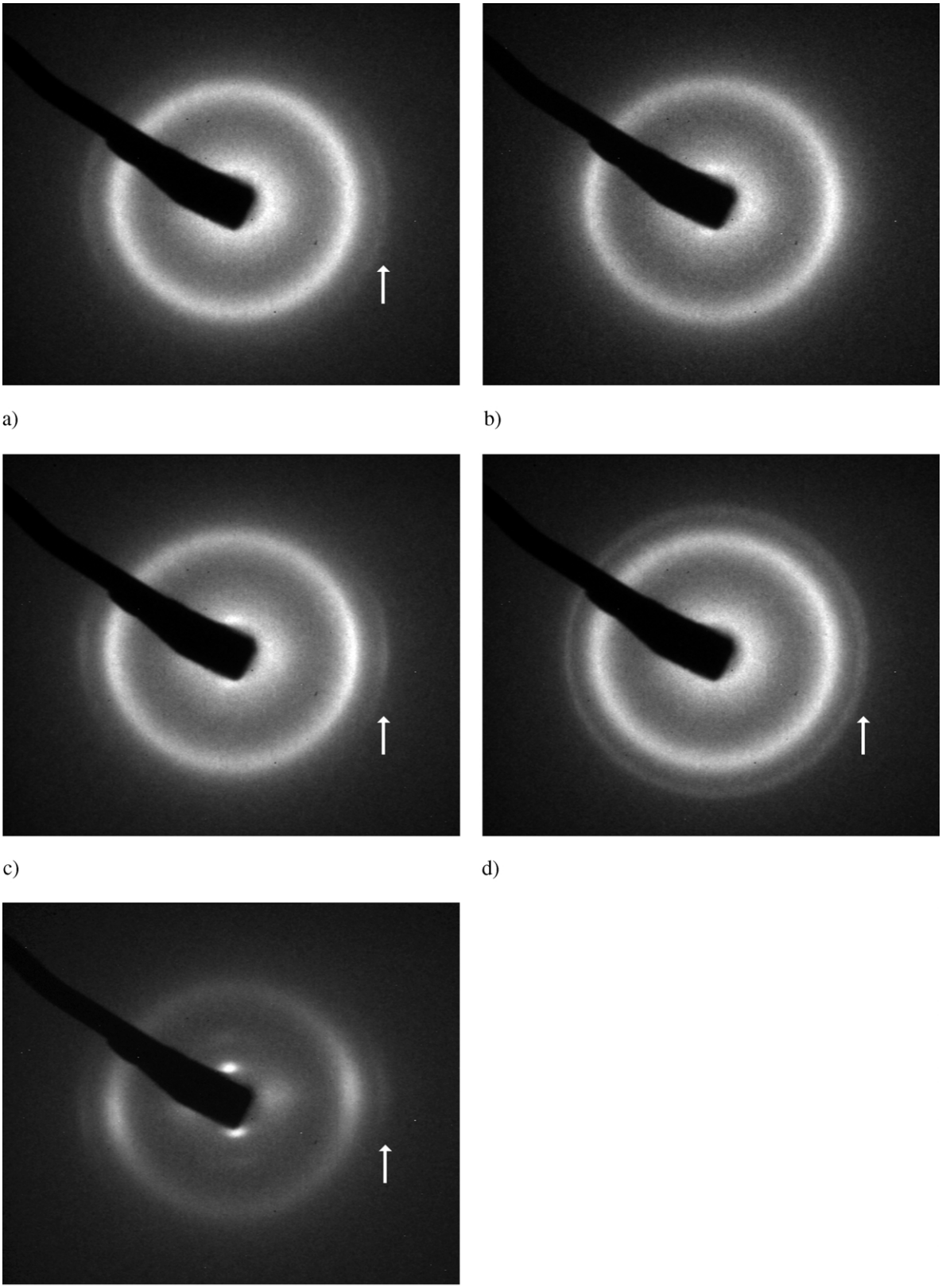

Fig. 5. X-ray fibre diffraction patterns for samples containing (a) 10 wt% CNF, (b) 10 wt% eCGNT, (c) 5 wt% aCGNT, and (d) 5 wt% AGNT. The patterns show a strong amorphous halo overlayed by a crystalline peak, and, at a distinctly larger scattering angle (marked by an arrow), a fainter ring or arcs associated with the (002) graphitic spacing within the nanofillers. A fibre diffraction pattern for the nanocomposite containing 5 wt% aCGNT strained to 100% is included in (e).

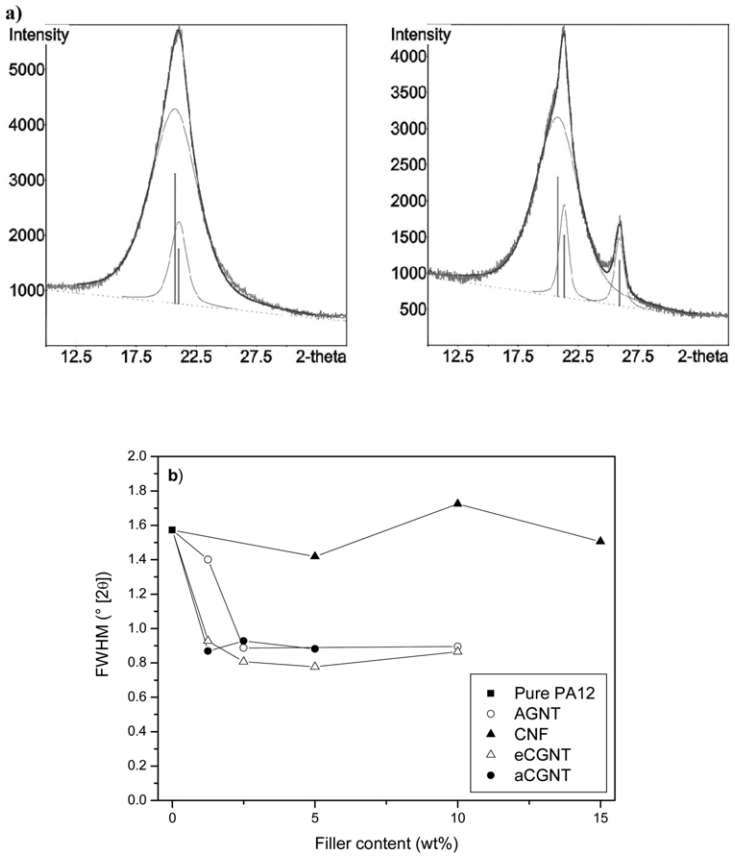

Fig. 6. (a) Equatorial X-ray line scans for pure PA12 fibres (left) and 5 wt% aCGNT nanocomposites (right), showing the peaks and bars indicating the relative areas of each of the peaks fitted to the amorphous halo, the main crystalline reflection and the (002) peak for the carbon. (b) Comparative plot of FWHM of crystalline polymer reflection for the various nanocomposites as a function of filler weight content.

limit since the orientation of the crystalline component is more significant than that of the amorphous halo.

Fig. 7(a) shows nonisothermal DSC thermograms obtained on as-spun nanocomposite fibres, at a scan rate of 10 °C/min from room temperature to 210 °C, as a function of aCGNT content. The curve for the pure polyamide-12 fibre is included as a comparison. Similar curves were obtained for all nanocomposite materials under investigation. As can be seen, there is a clear glass transition at around 50 °C which is not affected by the presence of the nanofiller. In addition, all curves display an endothermic peak above 170 °C which is associated with melting of the crystallites. Neither the melting peak temperature, the onset temperature to melting nor the shape of the peak shows significant variations between the pure polymer and the nanocomposites. Nevertheless, there appears to be a change in the heat capacity of all as-spun fibres between 100 °C and the onset to melting at around 170 °C, indicated by small deviations in the gradient. Such a broad crystallisation above T_g during a DSC experiment is common for polyamides and reflects the relaxation of processing stresses [29]. In the particular case of the aCGNT composites, shown in Fig. 7(a)), the appearance of a small exothermic shoulder prior to melting becomes more evident with increasing nanotube loading fraction. Again, a similar effect was observed for all the nanoscale fillers. Further analysis using 30 °C/min scans, shown in Fig. 7(b), more clearly reveals a combined melting and recrystallisation process during the heating of the pure polyamide-12 fibres which results in a second melting peak appearing at lower temperatures. For the nanocomposites, there appears to be an exothermic deviation from the baseline compared to the pure polymer, independent of loading fraction. Detailed cycling DSC studies provided further evidence for an exothermic process during heating of the as-spun fibres in the DSC, both for the pure polymer and the nanocomposites. In an attempt to establish a comparative degree of crystallinity of all nanocomposite fibres the total melting peak area was evaluated, normalised to the fraction of polymer present. This approach led to a roughly constant degree of crystallinity for all the samples between 23 to 27% (based on an enthalpy of melting of 209.34 J/g for 100% crystalline material [30]). Although, it seems that the nanofillers do not effect the maximum crystallinity that can be obtained, it must be noted that these results present a (potentially large) overestimation of the true, initial, degree of crystallinity of the as-spun fibres, due to the combined melting and recrystallisation processes taking place. The X-ray based estimate of initial crystallinity is likely to be more reliable.

Nonisothermal crystallisation studies were carried out by

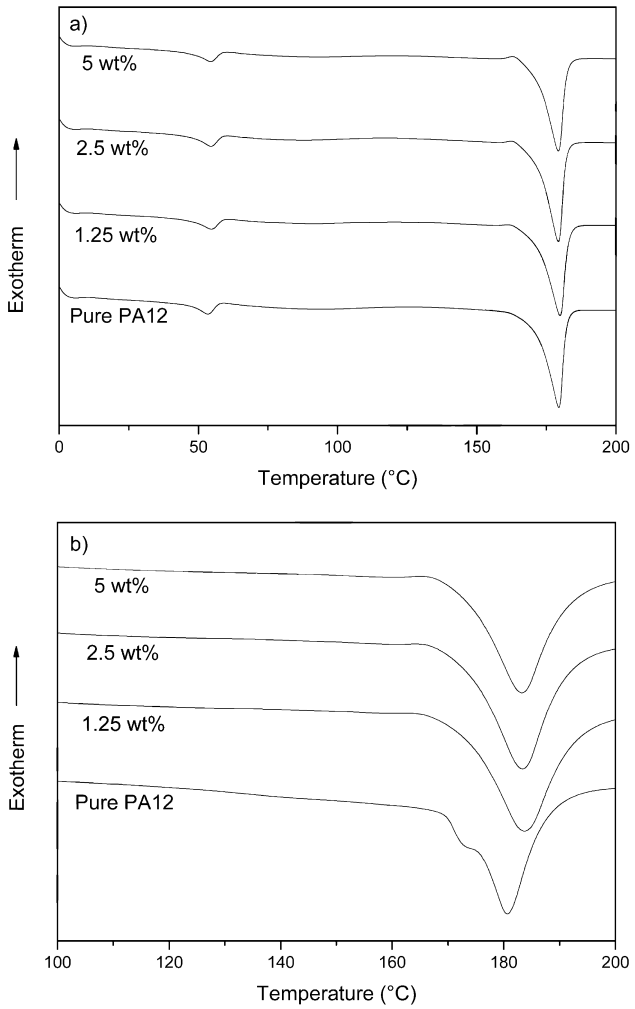

Fig. 7. DSC data obtained for aCGNT nanocomposite fibres, with increasing filler loading fraction, at (a) +10 °C/min, and (b) +30 °C/min.

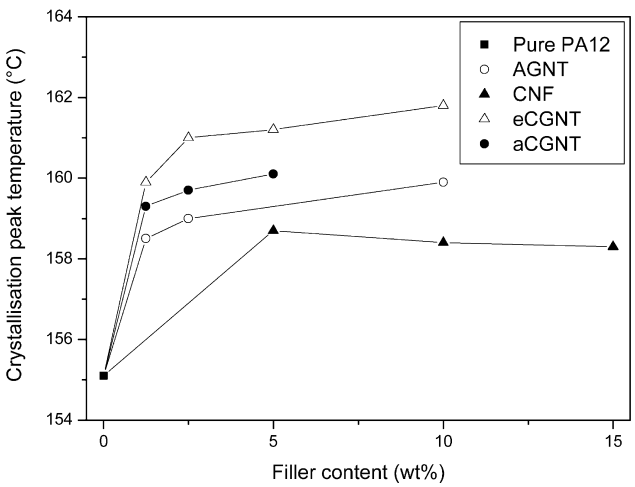

Fig. 8. Comparative plot of the crystallisation peak temperature at −10 °C/min for all PA12 nanocomposite fibres as a function of filler weight content.

heating to 210 °C and holding for 5 min prior to cooling at 10 °C/min. A single narrow crystallisation peak at around 156 °C was observed for the pure polyamide-12 sample. As can be seen in Fig. 8, all the nanocomposites showed increased onset and peak crystallisation temperatures. Depending on the filler type, the peak became broader and decreased in intensity. These effects were most pronounced for the eCGNTs. In all cases, the nucleation effect is most prominent for low filler loading fractions below 5 wt%. An interpretation based on enhanced thermal conductivity might be possible, but would not explain the plateau behaviour above 5 wt%.

A typical set of tensile engineering stress–strain curves of nanocomposite fibres containing the entangled and the aligned multi-wall carbon nanotubes is shown in Fig. 9. As indicated by the curves, the pure polymer and many of the nanocomposites revealed a two-stage yielding behaviour between about 3 and 30% of strain, followed by a stress plateau up to about 190% strain corresponding to drawing (it should be remembered that the data were obtained under force control, hence no 'yield-drop' could occur). The

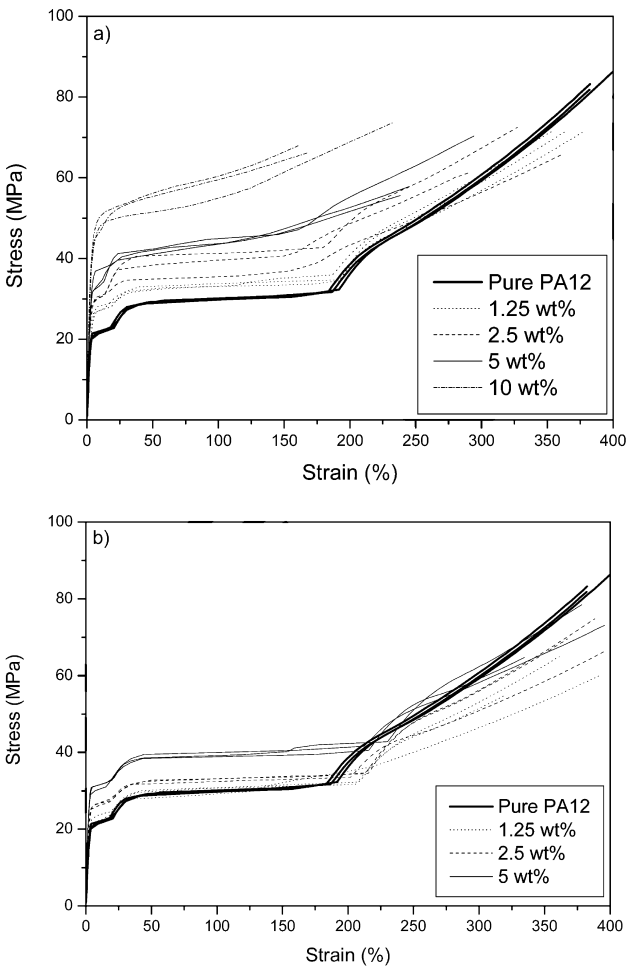

Fig. 9. Nominal stress–strain curves with increasing filler weight content obtained under stress control at 30 °C for nanocomposite fibres containing (a) eCGNT and (b) aCGNT.

occurrence of the characteristic two-stage yielding behaviour could be seen for all nanocomposites up to a filler concentration of 5 wt% (10 wt% in case of the carbon nanofibres). At higher filler loading fractions the tensile behaviour changed to a simple yielding, followed by a steady stress increase.

The data in Fig. 9 further show a general trend for a slight reduction in the slope of the stress–strain curves in the plastic deformation regime (following the drawing of the fibres) for the nanocomposites compared to the neat PA12. Unfortunately, the maximum strain of the apparatus did not lead to failure of all the samples, hence a conclusive analysis of ultimate strength is not possible. Nevertheless, the ultimate elongation of the nanocomposites appeared to decrease with increasing filler content, but by an amount that depended on the filler type. Notably, the aCGNT had little impact on ultimate elongation, but the eCGNT reduced it significantly. In addition, the first yield strain appeared unaffected by the both filler type and loading fraction whereas the second yield strain was reduced with increasing filler loading fraction for all filler types. In all cases, the yield stress increased with increasing filler loading fraction.

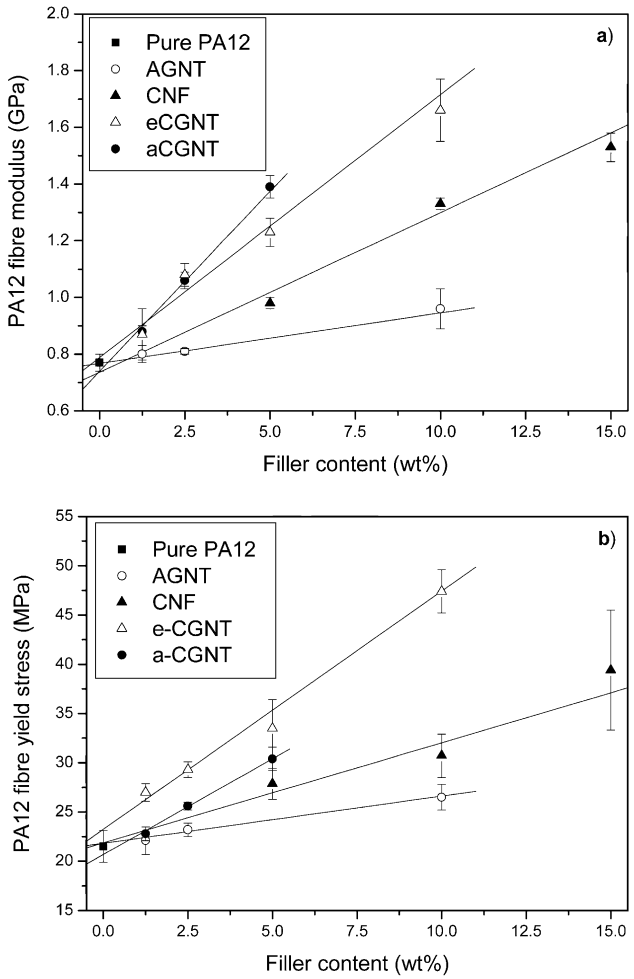

Fig. 10. Plots summarising the relationship between nanoscale filler weight content and (a) tensile modulus and (b) yield stress.

Fig. 10(a) shows a comparative plot of the fibre tensile modulus as a function of filler weight fraction, clearly revealing linear increases in nanocomposite stiffness for all filler types. The moduli were calculated for the initial, elastic portion of the stress–strain curves, before necking occurs. As can be seen, the aCGNTs show the steepest increase in composite stiffness, closely followed by the eCGNTs. The AGNTs present the worst increase in nanocomposite stiffness; a result that can be attributed to their poor dispersion and alignment. The yield stress data showed similar trends with both the eCGNTs and aCGNTs revealing the most prominent increases as a function of filler weight content; see Fig. 10(b). It is interesting to note that the performance increase was slightly higher for the entangled nanotubes than the aligned nanotubes, in this case.

4. Discussion

It is important that the new results on nanotube composites are set in the context of other, more established, nanocomposites. Clay-containing, nanocomposites, which are frequently based on polyamides, have received widespread attention due to the possibility of tailoring their strength/stiffness/toughness balance as well as improving the thermal stability, fire retardance, and gas barrier characteristics. Recently, nanoclay-reinforced polyamide-6 fibres have been produced, in this case for fire retardant textiles [31]. Many of the issues relating to nanotube composites are reflected in the existing work on nanoclay systems.

4.1. Matrix morphology

In general, the presence of modifier particles, even at low loadings, influences the crystallization behaviour of semi-crystalline polymer matrices. The development of polymorphism, for example, is a common effect in polyamide-6 layered silicate nanocomposites which has been assigned to a heterogeneous nucleation on the silicate particles [32,33]. Polyamide-12 usually crystallises in the γ-form from the melt at atmospheric pressure, even if melt-spun into monofilaments [34]. This crystal structure is believed to be hexagonal or monoclinic with two strong WAXS reflections corresponding to *d* spacings of about 0.42 and 1.59 nm. On the other hand, certain conditions such as solution-casting or high pressures can favour the monoclinic α-structure which is characterised by d spacings of about 0.37 and 0.45 nm [35]. A coexistence of the two crystal structures has also been observed in solution-cast polyamide-12 films, verified by WAXS [36].

The X-ray patterns shown in Figs. 5 and 6 indicate the presence of the γ-structure in all of the melt-spun nanocomposites. No reflections corresponding to the α-form could be distinguished. The development of strong meridional reflections at low angles in the 2D-patterns of a

strained sample shown in Fig. 5, further verifies the γ-structure assignment [37]. The single melting peak observed in the DSC thermograms shown in Fig. 7 at a low heating rate also confirms the absence of any polymorphism in these samples, in agreement with both biaxially-oriented, pure polyamide-12 films [38] and polyamide-12 based silicate nanocomposites [39,40]. In contrast, the presence of carbon nanotubes has been reported to induce polymorphic behaviour in polyvinylidiene difluoride [41] and unoriented polypropylene films [16].

4.2. Crystallisation behaviour

The nonisothermal DSC thermograms revealed a heteronucleation effect associated with the nanoscale fillers investigated in this study. Similar effects have been observed for silicate particles dispersed in polyamide-6 [33], polyamide-12 [39], and polyamide-66 [42]. In these studies, the nucleation effect was found to be most prominent for small filler loading fractions [33,42], in agreement with our data summarised in Fig. 8. Similar nucleation effects as a function of filler loading have been observed in recent studies of a semicrystalline polypropylene containing vapour-grown carbon nanofibres [15] as well as single-wall carbon nanotubes [18]. Fig. 8 also provides evidence that the degree of heteronucleation follows the trend of increasing surface area (reducing diameter) of the carbon nanotubes for a given concentration of catalytically-grown material. The AGNTs stimulated relatively little heteronucleation, as might be expected from their poor dispersion and their dilution by relatively large, contaminating graphite particles.

4.3. Orientation

The orientation of the CNFs and the aCGNTs with respect to the fibre axis can be quantitatively assessed from the 2D WAXS patterns. Integrated intensities around the (002) reflection as a function of azimuthal angle for the as-spun nanocomposites and the nanocomposite strained to 100% were fitted with a Gaussian function. The resulting FWHM of the Gaussian fits as a function of filler loading fraction are summarised in Table 1. The quality of the 2D X-ray pattern and the overlap of the amorphous halo and crystalline reflection of the polyamide-12 matrix intimates against a complex integration to determine the crystalline orientation.

Table 1
Comparative evaluation of orientation of the graphitic (002) spacing in PA12 nanocomposites containing well-dispersed CNF and aCGNT

Nanocomposite type	Filler content (wt%)	FWHM (002) (°)
As-spun PA12-CNF nanocomposites	5	56.8
	10	62.4
	15	59.7
As-spun PA12-aCGNT nanocomposites	2.5	27.2
	5	29.8
PA12-aCGNT nanocomposite strained to 100%	5	30.1

In the case of the aCGNTs, an average degree of alignment of about $\pm 15^{\circ}$ to the fibre axis was achieved, independently of filler content, within experimental accuracy. The alignment of the CNFs is about $\pm 30^{\circ}$, although it should be noted that the apparent lower orientation of the CNF is partly due to the graphitic planes in the inner part of the nanofibre wall which are arranged in the 'herringbone' structure at $\pm 15^{\circ}$ with respect to the tube axis; hence the overall alignment of the fibre/tube axes is probably similar for these two fillers. This analysis highlights the quality of alignment that can be achieved by melt-spinning of nanocomposite fibres containing well-dispersed carbon nanofibres and nanotubes. Interestingly, comparison of as-spun and cold drawn samples demonstrates that drawing of such nanocomposite fibres does not induce further alignment. This result suggests that the nanomaterials are already fully aligned by the relatively modest melt draw ratio used in this study. The apparent remaining misorientation then reflects the intrinsic 'waviness' of the nanofillers and the misorientation of the graphitic layers due to disorder.

Qualitatively, the degree of alignment observed for the dispersed nanoscale fillers in this study is similar to results obtained for CNFs in other thermoplastic matrix nanofibre composites [13,21], although in polypropylene, the superposition of the graphitic and polymer peaks make a comparison difficult [11]. However, as-spun, the alignment of the polymer crystallites is poorer in the PA-12 nanocomposites than in the literature systems, due to a lower draw ratio in the melt; after cold drawing, the polymer alignment is similar. Increasing the filler concentration of CNFs up to 15 wt% does not decrease the filler alignment as has been observed for extruded nanofibre-polypropylene strands [4].

4.4. Degree of crystallinity

The degree of matrix crystallinity, estimated from the DSC experiments, of around 25% for the nanocomposite fibres, is in agreement with similar studies of both biaxially oriented pure PA-12 films [38] and extruded PA-12 layered silicate nanocomposites [39]. Although, as discussed above, these values are an upper limit for the true degree of crystallinity of the as-spun fibres due to the combined melting and recrystallisation processes during the DSC runs [29]. Similar deviations from the baseline between the glass transition and the melting endotherm were observed in the case of the pure films [38] and nanocomposites [39]. On the other hand, the nonisothermal heating thermograms, as well as the cycling studies, revealed no significant changes in the magnitude of the enthalpies related to the matrix reorganisation as a function of filler type and loading fraction,

suggesting that the degree of crystallinity is reasonably constant across all of the samples both as-spun and after annealing.

Analysis of the X-ray patterns also allows the determination of the degree of matrix crystallinity of as-processed samples. Although the results are an overestimate due to the anisotropy of the samples, the degree of crystallinity again appears to be constant, within error, regardless of filler content. On the other hand, the addition of small amounts of nanofiller, up to around 2.5 wt%, reduces the width of the crystalline peak (Fig. 6(b)), suggesting an increase in crystallite size. It is known that polyamides obtained by fast cooling processing methods, such as the one used in this study, tend to develop smaller crystallite dimensions that broaden the crystalline peaks in X-ray patterns [29]. The increase in crystallite size matches the heteronucleation effect of the nanofillers, with the larger surface area nanotubes having the biggest influence. One simple explanation may be that early nucleation leaves more space for the heteronucleated crystals to grow before homonucleation within the rest of the matrix leads to impingement.

4.5. Mechanical properties

Filler dispersion, aspect ratio, and orientation are crucial factors in determining the mechanical properties of particle-filled polymers. The exact determination of these factors becomes more difficult with decreasing size of the particles, and hence a full analytical investigation of the intrinsic filler properties of the kind developed for short-fibre composites is not yet possible; however, some simple analysis can be attempted.

The prediction of the elastic properties of short-fibre reinforced polymers is a well-investigated topic. O'Regan et al. compared the predictions of the three most common models to experimental data on injection-moulded short-glass-fibre polyamide-6 composites and showed that the closest match was achieved using the Krenchel rule-of-mixtures approach [43]. The modified Krenchel [44] rule-of-mixture for the composite modulus parallel to the principal fibre axis is given by:

$$E = \eta_0 \eta_1 V_f E_f + (1 - V_f) E_m \quad (1)$$

Here, E_f and E_m are the fibre and matrix elastic moduli, V_f is the fibre volume fraction, and η_0 and η_1 are efficiency factors relating to the orientation and length of the reinforcing fibres, respectively. In the absence of significant differences in the polymer matrix morphology as a function of filler type and content, the increase in tensile stiffness of the as-spun polyamide-12 nanocomposites can be assessed using this simple rule-of-mixture approach. However, the accurate determination of the filler volume fraction is complicated by the need to estimate the purity and intrinsic density of the filler particles. The effective particle density depends on the size of the central cavity that remains unfilled, the quality of the dispersion and whether the polymer has fully penetrated remaining particle clusters. Lastly, the large surface areas associated with nanoparticles mean that any interfacial variations in polymer morphology can lead to variations in matrix density. Therefore, it is more straightforward to evaluate the nanocomposite performance as a function of weight fraction. The trends remain linear because the densities of the fillers are relatively similar to that of the matrix and their loading fractions relatively low; hence the relationship between volume and weight fraction is extremely close to linear over the range under consideration. Therefore, substituting weight fraction for volume fraction in Eq. (1) and using the weight-based gradients of the data shown in Fig. 10(a), effective moduli, $\eta_0 \eta_1 E_f$, of the various carbon nanostructures were obtained, as shown in Table 2. The effective moduli for the carbon nanomaterials, based on weight fraction, are underestimates of the normal volume fraction based value, by a multiple of approximately 0.74, although the exact figure will vary with filler type and its (unknown) effective density. For comparison, equivalent data deduced from literature reports for commercial clay nanoparticles, as well as short glass and carbon fibre filled polyamides are included.

The melt-spun polyamide-12 nanocomposites containing the aCGNTs reveal the highest effective modulus, closely followed by the eCGNTs. The CNFs show intermediate results between the CVD-grown nanotubes and the arc-grown material. The aCGNTs and the CNFs showed very similar levels of dispersion and alignment; the alignment of the eCGNT is less certain due to the diffuse X-ray signal and the presence of a small number of aggregates within the matrix. Nevertheless, the greater stiffening effect of the aCGNTs compared to the eCGNT is expected, due to their lower 'waviness' and greater crystallinity as seen in Raman spectroscopy. If anything, a larger distinction might be anticipated; however, the larger surface area of the eCGNTs may increase polymer constraint and hence mitigate their other disadvantages. The better performance of the CVD-grown multi-wall carbon nanotubes compared to the CNFs is not surprising, given the more favourable orientation of the graphitic planes and the lower defect concentration. The large number defects in the outer layers of the CNF structure might strengthen the polymer matrix-filler interface but will reduce the intrinsic stiffness of the nanofibres. The low effective stiffness of the arc-grown material on the other hand is disappointing, given their high intrinsic crystalline quality. However, the combination of low purity and poor dispersion means that the effective loading fraction is rather low. Calculation of the intrinsic carbon nanotube/nanofibre modulus E_f is not meaningful without knowing more accurately the degree of orientation of the fibres (not the graphitic planes) and their aspect ratio (which may be degraded by processing [13]).

The effective moduli of about 10 and 13 GPa for the two CVD-grown nanotube materials are almost twice as high as those achieved for injection-moulded polyamide-12 clay

Table 2
Comparative evaluation of effective modulus of various nanoscale fillers in polyamide nanocomposites

Nanocomposite type and processing	Filler type	Loading fraction (wt%)	Effective modulus $\eta_0\eta_L E_f$ (GPa)	Reference
Melt-spun polyamide-12 fibres containing various carbon nanostructures				
	Vapour-grown carbon nanofibres	0–15	5.0–6.4	This work
	Aligned CVD-grown multi-wall carbon nanotubes	0–5	9.6–13.2	
	Entangled CVD-grown multi-wall carbon nanotubes	0–10	8.8–13.2	
	Arc-grown multi-wall carbon nanotubes	0–10	2.4–3.2	
Polyamide-12 melt-blended clay nanocomposites				
Extruded + injection moulded	Tetrasilisic fluoromica	0 and 4	6.8	[39]
Extruded	Tetrasilisic fluoromica	0–4	7.4–7.6	[40]
Polyamide-6 melt-blended clay nanocomposites				
Extruded + hot-pressed	Organoclay	0–10	12.7–21.5	[32]
Extruded + injection moulded	Montmorillonite	0 and 5	16.2	[45]
Extruded + injection moulded	Montmorillonite	0 and 3	60.1	[46]
Electrospun fibres	Organoclay	0–5	20.5–30.5	[47]
Polyamide-6 melt blended short-fibre composites				
Extruded + injection moulded	E-glass fibres, 6 mm long	0–30	11.5–12	[46]
Extruded + injection moulded	C-fibres, 6 mm long	0–30	18.8–27.6	

nanocomposites. The CNF and clay PA-12 systems have similar stiffnesses. The best results achieved with carbon nanotubes in the polyamide-12 matrix are also comparable to those typically observed for melt-blended polyamide-6 clay nanocomposites [32,45]; although there is a report of significantly greater stiffness for clay in PA-6 [46]. The problems, mentioned above, of accurately determining the key factors, such as filler dimensions, orientation and arrangement, are common to all these nanocomposites. Hence the effective moduli are a reasonable means of comparing the current level of stiffening available. Although the processing conditions and type of samples vary, all will have experienced a degree of shear alignment during processing. Few papers discuss the mechanical properties of nanocomposite polymer fibres. One example [47] uses electrospinning to produce highly aligned fibres of previously melt-blended nanoclay-PA6 composites. The effective moduli are only modestly higher than the injection-moulded samples, suggesting that, in the latter case, the alignment of the clay platelets may already be quite reasonable.

Comparing the effective modulus of the CVD-grown multi-wall carbon nanotubes to those of short glass and carbon fibres one can see that the performance of the nanotubes is similar to that of the glass fibres but only half that of carbon fibres, even though the nanotubes are likely to be more aligned. Although the intrinsic moduli experimentally observed for high-temperature grown multi-wall carbon nanotubes, between 270 and 950 GPa [48], are similar to common carbon fibre grades, it has been verified experimentally that multi-wall carbon nanotubes grown at lower temperatures have a significantly lower intrinsic nanotube modulus [3,49]. Furthermore, multi-wall carbon nanotubes exhibit a so-called intrinsic 'waviness' as a result of their structural defects which leads to a curved appearance of the filler in the polymer host. Finite element analysis of this issue has shown that the effective nanotube modulus decreases dramatically for such curved nanotubes [23,24]. Intrinsic 'waviness' is also present in carbon nanofibres.

A comparison to literature values for other as-spun carbon nanofibre-reinforced polymer composite fibres shows that the effective nanofibre moduli obtained in this study appear relatively low. However, the values of roughly 25–60 GPa that can be deduced from the literature may be misleading. In the case of a PET matrix [13], the stiffness increase due to the CNF is small compared to the relatively high modulus of the heavily-drawn matrix and is less than the quoted errors. In studies of CNF-reinforced polypropylene fibres [9,11], the influence of the nanoscale filler on the polymer morphology was not investigated. The nonlinear increase in composite modulus with increasing filler content might indicate a significant variation in both the crystal structure and/or the degree of crystallinity of this matrix system [14–18]. The effective nanofibre modulus of the PA-12 system compares more favourably with a recent study of as-spun carbon nanofibre-reinforced poly(ether ether ketone) fibres where nanofibre-induced changes in the degree of crystallinity were clearly observed and taken into account [21]. Nevertheless, it is possible that differences in the type of CNF used or their interactions with other polymer systems might have raised the intrinsic modulus or shortened the stress-transfer length, leading to a rise in effective modulus. In any case, the initial stiffening effect of small additions of single-walled nanotubes to polypropylene fibres dwarfs the impact of CNFs but seems to saturate at loading fractions as low as 1–2 wt% [10]. The single-walled nanotubes are intrinsically more perfect and have a

flexibility that allows them to align to the fibre axis; the saturation effect is not yet fully understood, although a similar trend has been observed in nanoclay composites.

The stress–strain curves of the as-spun polyamide-12 nanocomposites shown in Fig. 9 reveal a two-stage yielding process for the pure PA12 matrix and the nanocomposites containing low filler contents. The first stage of the yielding process consists of the formation of a neck at the first stress plateau. This onset to plastic deformation is immediately followed by strain-induced crystallisation and orientation of the crystalline phase with respect to the fibre axis. The resulting stiffening of the neck region leads to the propagation of the neck to both clamped ends of the fibres. This secondary drawing stage, converting the microstructure into a fibrillar morphology, appears as a long plateau due to the force-control nature of the tensile test. This two-stage deformation process is not affected up to nanoscale filler contents of 5 wt%, although the stress increases with increasing weight fraction. At filler weight fractions above 5 wt% a transition to a one-stage yielding occurs. This transition must arise from limitations in molecular mobility at these higher filler concentrations, which raises the initial yield stress to the level at which secondary drawing can occur. It is, therefore, not surprising that the entangled multi-wall carbon nanotubes lead to the highest yield stresses in the nanocomposite fibres. The entanglement state and close proximity of these nanotubes, shown in Figs. 1 and 2, and highlighted by the surface area dependent phenomena discussed above, most effectively reduce the mobility of the matrix and its deformability.

It is interesting to note that the pure PA12 fibres show the steepest stress increase during cold drawing and ultimately attain the highest strength. The greater relative improvement of the pure polymer fibres is to be expected given the lack of further improvement in nanofiller orientation during the drawing process. However, the higher absolute ultimate strength of the pure PA-12 fibres compared to the nanocomposites, is disappointing. The reduction in ultimate elongation can be attributed to interactions between the nanotubes and the constraint of the polymer in the interfacial region; unsurprisingly, the eCGNTs that are both entangled and have a high surface area lead to a dramatic reduction in draw ratio, whereas the aCGNTs have little effect. The presence of filler aggregates could also provide defect sites to initiate failure. Constraint of the matrix may prevent optimal orientation and crystallinity developing, as well as hindering microvoid formation, leading to a reduction in ultimate strength. However, at a fundamental level, the carbon nanofillers are not providing the strengthening effect that was hoped for. Possible explanations include the poor intrinsic quality of catalytically-grown multi-walled materials, and the difficulties of stress transfer, either from matrix to filler, or internally within the nanotube structure. The reduction in strength is in contrast to clay-reinforced polyamide-12 nanocomposites, where the improved strength is attributed to an enhanced microvoid formation ability [39]. Improvements have also been observed in single-walled nanotube [10] and CNF [9, 11] filled polypropylene although, again, the matrix morphology is uncertain. No improvements were observed for CNF in PET [13].

In the context of this comparative study, it is interesting to speculate as to what the ideal nanotube structure for reinforcement might be. The choice of ideal diameter is complex. Very small diameters, particularly single-walled nanotubes, are relatively flexible, potentially leading to lower viscosities and greater robustness during processing, but also persistent entanglements. The higher the surface area, the greater the impact of the nanotubes on matrix morphology; effects may or may not be beneficial and will depend on the polymer used. For the smallest nanotube sizes, where the diameters of the nanotubes and polymer molecules are similar, particulate concepts such as heterogeneous nucleation may no longer be helpful. The composite is essentially a polymer-polymer blend, although a rather unusual one which may give rise to new behaviours. One major difficulty with small diameter nanotubes is that they become increasingly difficult to wet. By trivial estimation, even a 1 vol% loading of single-walled nanotubes ensures that all of the polymer molecules are within one radius of gyration (say 5 nm) of a nanotube. This result implies that complete wetting of high loading fractions of single-walled nanotubes will be difficult, at least by conventional means, and that even more modest concentrations may be brittle and hard to process due to the constraint of the polymer. Alternative approaches, based on layer-by-layer assembly and lyotropic spinning of single-walled nanotube solutions have already been explored and may prove to be important. However, for the purposes of simple, thermoplastically-processed composites, intrinsically straight, highly crystalline, multi-walled nanotubes might be expected to yield the best mechanical properties, as long as internal shear failures can be minimised. It remains to be seen whether there is an optimal defect concentration that prevents internal sliding without harming the intrinsic properties excessively. Small diameter multi-wall nanotubes (less than perhaps 5 nm) may prove to be the ideal material for mechanical reinforcement, providing balance between the relevant factors.

5. Conclusions

This study has successfully explored the potential of various multi-wall carbon nanotubes and nanofibres as mechanical reinforcements in polyamide-12 composite fibres. Using as-produced nanomaterials, filler loading fractions of up to 15 wt% were realised, by following thermoplastic processing techniques to produce melt-spun nanocomposites. The vapour-grown carbon nanofibres and CVD-grown multi-wall carbon nanotubes dispersed well into the matrix and provided linear increases in initial stiffness and yield strength, as a function of loading fraction.

In contrast, the use of unpurified arc-grown material led to defective composites and comparatively low increases in performance. A detailed investigation of the matrix morphology demonstrated that the nanofillers act as heteronucleation sites for crystallisation under slow cooling conditions, the effect being most pronounced for low filler concentrations and small nanotube diameters. However, the outcome was a uniform degree of crystallinity with deviations only in crystallite size. The increase in stiffness was, therefore, evaluated in terms of an effective filler modulus; the largest value was obtained for the aligned CVD-grown multi-wall carbon nanotubes. This effective modulus is higher than that found in melt-blended organoclay-polyamide-12 nanocomposites. However, the nanotube moduli are lower than for short carbon or glass fibres in polyamides and than for single-walled nanotubes in polypropylene. The discrepancy probably relates to the intrinsic crystalline quality of the catalytic nanotubes and the waviness of embedded nanotubes within the polymer host.

Surprisingly, subsequent cold drawing did not induce further improvements in nanomaterial alignment. This result implies that these nanotubes orient rather easily under shear flows, but have significant in-built curvature from their synthesis, which cannot be straightened. The constraint of the polymer matrix during cold drawing due to the high surface area of the nanofiller and its nucleating effect, prevent the evolution of the optimal polymer microstructure, leading to a reduction in ultimate strength. Hence, improved properties of these nanocomposites may be generated by maximising the draw ratio at higher temperatures. In situ X-ray studies during both hot and cold drawing would be very illuminating. To conclude, over recent years, it has clearly been demonstrated that useful mechanical and functional property benefits can arise from adding nanotubes to thermoplastic polymers. Continued exploration of such systems containing both single- and multi-walled materials should prove fruitful.

Acknowledgements

The authors would like to thank the National Centre for Biomedical Sciences in Ireland and DSM for the use of their equipment and Prof. J.-B. Nagy (Namur) for the supply of nanotube material. Financial support from the EC Thematic Network ‘CNT-NET’ [G5RT-CT-2001-05026], the EPSRC, and the Cambridge European Trust is gratefully acknowledged.

References

[1] Thostenson ET, Ren ZF, Chou TW. Advances in the science and technology of carbon nanotubes and their composites: a review. Comp Sci Tech 2001;61:1899–912.

[2] Lau K-T, Hui D. The revolutionary creation of new advanced materials-carbon nanotube composites. Composites: Part B 2002;33: 263–77.

[3] Salvetat J-P, Kulik AJ, Bonard J-M, Briggs GAD, Stöckli T, Méténier K, Bonnammy S, Béguin F, Burnham NA, Forró L. Elastic modulus of ordered and disordered multiwalled carbon nanotubes. Adv Mater 1999;11(2):161–5.

[4] Kuriger RJ, Alam MK, Anderson DP, Jacobsen RL. Processing and characterization of aligned vapor grown carbon fiber reinforced polypropylene. Composites: Part A 2002;33(1):53–62.

[5] Jin L, Bower C, Zhou O. Alignment of carbon nanotubes in a polymer matrix by mechanical stretching. Appl Phys Lett 1998;73(9):1197–9.

[6] Thostenson ET, Chou T-W. Aligned multi-walled carbon nanotube-reinforced composites: processing and mechanical characterisation. J Phys D: Appl Phys 2002;35:77–80.

[7] Safadi B, Andrews R, Grulke EA. Multiwalled carbon nanotube polymer composites: synthesis and characterization of thin films. J Appl Polym Sci 2002;84:2660–9.

[8] Haggenmueller R, Gommans HH, Rinzler AG, Fischer JE, Winey KI. Aligned single-wall carbon nanotubes in composites by melt processing methods. Chem Phys Lett 2000;330(3–4):219–25.

[9] Gordeyev SA, Ferreira JA, Bernado CA, Ward IM. A promising conductive material: highly-oriented polypropylene filled with short vapour-grown carbon fibres. Mater Lett 2001;51(1):32–6.

[10] Kearns JC, Shambaugh RL. Polypropylene fibers reinforced with carbon nanotubes. J Appl Polym Sci 2002;86(8):2079–84.

[11] Kumar S, Doshi H, Srinivasarao M, Park JO, Schiraldi DA. Fibers from polypropylene/nano carbon fiber composites. Polymer 2002;43: 1701–3.

[12] Kumar S, Dang TD, Arnold FE, Bhattacharyya AR, Min BG, Zhang X, Vaia RA, Park C, Adams WW, Hauge RH, Smalley RE, Ramesh S, Willis PA. Synthesis, structure, and properties of PBO/SWNT composites. Macromolecules 2002;35(24):9039–43.

[13] Ma H, Zeng J, Realff ML, Kumar S, Schiraldi DA. Processing, structure, and properties of fibers from polyester/carbon nanofiber composites. Comp Sci Tech 2003;63(11):1617–28.

[14] Bhattacharyya AR, Sreekumar TV, Liu T, Kumar S, Ericson LM, Hauge RH, Smalley RE. Crystallization and orientation studies in polypropylene/single wall carbon nanotube composite. Polymer 2003; 44:2373–77.

[15] Lozano K, Barrera EV. Nanofiber-reinforced thermoplastic composites. I. Thermoanalytical and mechanical analyses. J Appl Polym Sci 2001;79(1):125–33.

[16] Grady BP, Pompeo F, Shambaugh RL, Resasco DE. Nucleation of polypropylene crystallization by single-walled carbon nanotubes. J Phys Chem B 2002;106(23):5852–8.

[17] Assouline E, Lustiger A, Barber AH, Cooper CA, Klein E, Wachtel E, Wagner HD. Nucleation ability of multiwall carbon nanotubes in polypropylene composites. J Polym Sci B: Polym Phys 2003;41: 520–7.

[18] Valentini L, Biagiotti J, Kenny JM, Santucci S. Morphological characterization of singe-walled carbon nanotubes-PP composites. Comp Sci Tech 2003;63:1149–53.

[19] Cadek M, Coleman JN, Barron V, Hedicke K, Blau WJ. Morphological and mechanical properties of carbon-nanotube-reinforced semicrystalline and amorphous polymer composites. Appl Phys Lett 2002;81(27):5123–5.

[20] Sandler J, Werner P, Shaffer MSP, Demchuk V, Altstädt V, Windle AH. Carbon-nanofibre-reinforced poly(ether ether ketone) composites. Composites: Part A 2002;33(8):1033–9.

[21] Sandler J, Windle AH, Werner P, Altstädt V, Es MV, Shaffer MSP. Carbon-nanofibre-reinforced poly(ether ether ketone) fibres. J Mater Sci 2003;38(10):2135–41.

[22] Marcinčin A. Modification of fiber-forming polymers by additives. Prog Polym Sci 2002;27:853–913.

[23] Fisher FT, Bradshaw RD, Brinson LC. Effects of nanotube waviness

on the modulus of nanotube-reinforced polymers. Appl Phys Lett 2002;80(24):4647–9.
[24] Fisher FT, Bradshaw RD, Brinson LC. Fiber waviness in nanotube-reinforced polymer composites-I: modulus predictions using effective nanotube properties. Comp Sci Tech 2004; in press.
[25] Cadek M, Murphy R, McCarthy B, Drury A, Lahr B, Barklie RC, in het Panhuis M, Coleman JN, Blau WJ. Optimisation of the arc-discharge production of multi-walled carbon nanotubes. Carbon 2002; 40:923–8.
[26] Singh C, Shaffer MSP, Windle AH. Synthesis of aligned films of carbon nanotubes. Carbon 2003;41(2):359–68.
[27] Hernadi K, Fonseca A, Piedigrosso P, Delvaux M, Nagy JB, Bernaerts D, Riga J. Carbon nanotubes production over Co/silica catalysts. Catal Lett 1997;48:229–38.
[28] Shaffer MSP, Windle AH. Fabrication and characterization of carbon nanotube/poly(vinyl alcohol) composites. Adv Mater 1999;11(11): 937–41.
[29] Khanna YP, Kuhn WP. Measurement of crystalline index in nylons by DSC: complexities and recommendations. J Polym Sci, Part B: Polym Phys 1997;35:2219–31.
[30] Gogolewski S, Czerniawska K, Gasiorek M. Effect of annealing on thermal properties of crystalline structure of polyamides. Nylon 12 (polylaurolactam). Colloid Polym Sci 1980;258(10):1130–6.
[31] Bourbigot S, Devaux E, Flambard X. Flammability of polyamide-6/clay hybrid nanocomposite textiles. Polym Degrad Stab 2002;75(2): 397–402.
[32] Liu TX, Liu ZH, Ma KX, Shen L, Zeng KY, He CB. Morphology, thermal and mechanical behavior of polyamide 6/layered-silicate nanocomposites. Comp Sci Tech 2003;63:331–7.
[33] Fornes TD, Paul DR. Crystallization behavior of nylon 6 nanocomposites. Polymer 2003;44:3945–61.
[34] Inoue K, Hoshino S. Crystal structure of nylon 12. J Polym Sci, Polym Phys Ed 1973;11:1077–89.
[35] Ishikawa T, Nagai S. Formation of α-nylon 12 by solution casting. J Polym Sci, Polym Phys Ed 1977;15:1315–7.
[36] Ishikawa T, Nagai S. Effect of casting conditions on polymorphism of nylon-12. J Polym Sci, Polym Phys Ed 1980;18:291–9.
[37] Northolt MG, Tabor BJ, van Aartsen JJ. Polymorphism in nylon 12. J Polym Sci: Part A-2 1972;10:191–2.
[38] Rhee S, White JL. Crystal structure and morphology of biaxially oriented polyamide 12 films. J Polym Sci B: Polym Phys 2002;40: 1189–200.
[39] McNally T, Murphy WR, Lew CY, Turner RJ, Brennan GP. Polyamide-12 layered silicate nanocomposites by melt blending. Polymer 2003;44:2761–72.
[40] Reichert P, Kressler J, Thomann R, Müllhaupt R, Stöppelmann G. Nanocomposites based on a synthetic layer silicate and polyamide-12. Acta Polym 1998;49:116–23.
[41] Carroll DL. Personal communication.
[42] Liu X, Wu Q, Berglund LA. Polymorphism in polyamide 66/clay nanocomposites. Polymer 2003;43:4967–72.
[43] O'Regan DF, Akay M, Meenan B. A comparison of Young's modulus predictions in fibre-reinforced polyamide injection mouldings. Comp Sci Tech 1999;59:419–27.
[44] Krenchel H. Fibre reinforcement. Copenhagen: Akademisk Forlag; 1964.
[45] Liu X, Wu Q, Berglund LA, Fan J, Qi Z. Polyamide 6-clay nanocomposites/polypropylene-grafted-maleic anhydride alloys. Polymer 2001;42:8235–9.
[46] Wu S-H, Wang F-Y, Ma C-CM, Chang W-C, Kuo C-T, Kuan H-C, Chen W-J. Mechanical, thermal and morphological properties of glass fiber and carbon fiber reinforced polyamide-6/clay nanocomposites. Mater Lett 2001;49(6):327–33.
[47] Giza E, Ito H, Kikuntani T, Okui N. Fiber structure formation in high-speed melt spinning of polyamide 6/clay hybrid nanocomposite. J Macromol Sci 2000;B39(4):545–59.
[48] Yu M-F, Lourie O, Dyer MJ, Moloni K, Kelly TF, Ruoff RS. Strength and breaking mechanism of multiwalled carbon nanotubes under tensile load. Science 2000;287:637–40.
[49] Pan ZW, Xie SS, Lu L, Chang BH, Sun LF, Zhou WY, Wang G, Zhang DL. Tensile tests of ropes of very long aligned multiwall carbon nanotubes. Appl Phys Lett 1999;74(21):3152–4.